**JOURNAL OF THEORETICAL AND APPLIED MECHANICS**
**62**, 1, pp. 143-156, Warsaw 2024
https://doi.org/10.15632/jtam-pl/176309

# STUDY ON DUCTILE FRACTURE CRITERION APPLIED TO SHEAR FRACTURE PREDICTION OF DP780 SHEET

Jiaxiong Wu, Xuguang Sun, Xiaoce Sun, Fu Chang
*China North Vehicle Research Institute, Beijing, China*
*corresponding author Xuguang Sun, e-mail: sun_xuguang@163.com*
Shudi Yang, Senqi Tan
*China North Artificial Intelligence and Innovation Research Institute, Beijing, China*

With the development of automotive lightweight technology, the improvement of the design of body sheet metal forming processes has gradually become a research focus. Advanced high--strength dual-phase steel is the main material for lightweight vehicle bodies, and exploring its accurate ductile fracture criteria plays an important role in predicting the forming fracture behavior of the sheet metal. The characterizations of the plastic behavior of the DP780 sheet before fracture were performed by the Swift hardening model. Three sets of tests from pure shear to tensile-shear stress states are designed to calibrate the ductile fracture parameters of Lou-Huh, Cockcroft-Latham, and Rice-Tracey criteria. The calibrated parameters are used to predict tensile shear test fractures and punching fractures at small bend fillets of molds. The results show the Lou-Huh criterion can accurately predict the shear fracture behavior of the DP780 sheet in the low-stress triaxiality (0.08-0.33).

*Keywords:* ductile fracture criterion, DP780, fracture prediction, shear fracture, sheet forming

## 1. Introduction

Based on the consideration of automobile lightweight, advanced high-strength steel DP780 has become the preferred material for body lightweight due to its high specific strength and good energy absorption (Zhou *et al.*, 2021). It is widely used in key parts such as the threshold beam, $B$ column, anti-collision beam, and ceiling beam. In 2002, the international iron and steel federation's "Advanced Automotive Concept for Ultra Light Steel Bodies (ULSAB-AVC)" project showed a high usage rate of 74% for DP steel in the body structure design. However, advanced high-strength steel also has a defect of poor room temperature formability. Therefore, to improve the formability of the sheet, a larger blank holder force or a smaller die-bending fillet is often used in the design of the stamping process, which results in shear fracture behavior of the DP780 sheet with no obvious necking before failure at the die bending fillet (Luo and Wierzbicki, 2010; Banabic *et al.*, 2020). The shear fracture of high-strength steel in the forming process is one of the main problems that hinder its application in automobile bodies. Traditional FLC curves and various criteria based on necking instability theory (Silva *et al.*, 2008) such as Swift dispersive instability theory (Swift, 1952), Hill concentrated instability theory (Hill, 1952), and the Marciniak-Kuczynski instability theory (Marciniak and Kuczynski, 1967), cannot accurately predict this type of shear fracture. In addition, the lack of accurate shear fracture criteria greatly limits the application of the sheet metal and forming process design. Therefore, from the perspective of industrial application, it is of great significance to explore the shear fracture criterion with an accurate prediction and a simple form to foresee the forming fracture of sheet metal.

The fracture of metal sheets evolved from micro-defects such as micro-dimples and micro--shear bands, and the evolution of the two types of micro-defects is controlled by the stress state (Li *et al.*, 2011b). The necking dominant fracture in a high-stress triaxiality region is related to continuous nucleation, growth and convergence of micro dimples, while the shear dominant fracture in the low-stress triaxiality region is caused by a continuous extension of micro cracks and micro holes into shear bands under shear action (Hu *et al.*, 2009). The researchers analyzed mechanical factors affecting the nucleation, growth, polymerization, and fracture of micro-voids in the material from the microscopic mechanism of ductile fracture (McClintock *et al.*, 1966; Puttick, 1959) and proposed many uncoupled ductile fracture criteria for predicting sheet-forming fracture (Rice and Tracey, 1969; Cockcroft and Latham, 1968; Oh *et al.*, 1979; Clift *et al.*, 1990). The above criteria mainly consider mechanical variables such as maximum normal stress, maximum shear stress and stress triaxiality, as well as combinations of mechanical variables. Nevertheless, due to the lack of research on a specific influence mechanism of mechanical variables selected in the criteria on the evolution of micro-defects, the stress state interval and fracture type applicable to the above criteria are different.

Based on the micro-mechanism theory, the criterion considering both the stress triaxiality and the Lode parameter has received extensive attention due to the wider range of applicable stress states. With a broad application of DP780 high-strength steel in the industry, it is of great research value to explore a more flexible and accurate ductile fracture criterion in forming simulation. In this paper, the advanced high-strength steel DP780 sheet is used as the research object. The stress and strain state parameters of the material in the low-stress triaxiality range are obtained by designing four kinds of unidirectional loading samples combined with numerical simulation. The parameters of Lou-Huh, Cockcroft-Latham, and Rice-Tracey ductile fracture criteria are calibrated, and then applied to fracture prediction of a tensile-shear test and shear fracture in stretch-bending forming of grooved parts in order to study their applicability and accuracy.

## 2. The test design and process

### 2.1. Sample design for different stress states

In this paper, the thickness of the advanced high-strength steel DP780 sheet sample is 1mm, and its chemical composition is shown in Table 1.

**Table 1.** Material chemical composition of the sample

| C | Si | Mn | P | S | Alt |
|---|---|---|---|---|---|
| 0.1 | 0.16 | 2.02 | 0.008 | 0.003 | 0.039 |

In order to analyze plasticity and fracture behavior of the DP780 sheet under low-stress triaxiality, four unidirectional loading specimens with different shapes and sizes are designed as shown in Fig. 1. The figure shows the uniaxial tensile specimen, pure shear specimen, 45° tensile shear specimen, and 60° tensile shear specimen, respectively.

### 2.2. The anisotropic test process

Three sets of uniaxial tensile specimens with different orientations are prepared by laser wire cutting to determine plastic anisotropy of DP78 sheets. The preparation orientations of laser wire cutting are 0°, 45° and 90° with the rolling direction, respectively. For the test method, the RDL50 universal testing machine is used to load the specimen with an elongation rate of 0.2 mm/min at room temperature. The loading process is quasi-static, and nominal stress-strain curve of the specimen gauge section can be obtained by an extensometer.

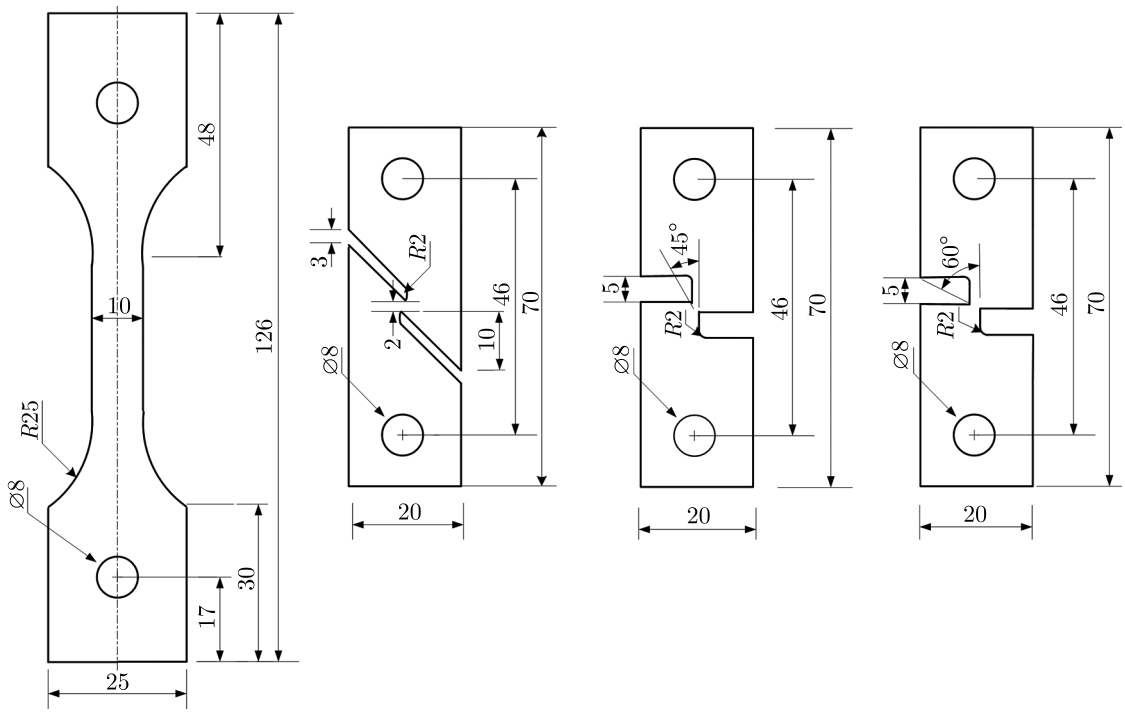


Fig. 1. Shape and size of the unidirectional loading sample

The equations for converting the nominal stress-strain curve into a real stress-strain curve are shown as follows

$$\varepsilon = \ln(1+\varepsilon_e) \qquad \sigma = \sigma_e(1+\varepsilon_e) \tag{2.1}$$

where $\sigma$ is the real stress, $\varepsilon$ is the real strain, $\varepsilon_e$ is the nominal strain, $\sigma_e$ is the nominal stress.

The real stress-true strain curves of the three orientations of the uniaxial tensile specimen can be obtained by the experimental results and Eqs. (2.1). The real stress-true strain curves are shown in Fig. 2. It can be seen from Fig. 2 that the true stress-strain curves of 0° and 45° orientations are consistent, and the real stress-true strain of 90° orientation is slightly higher by about 2%. The anisotropy characteristics of the DP780 sheet were not very obvious, and it could be assumed that the DP780 sheet had plane isotropy (Luo and Wierzbicki, 2010), so the von Mises yield criterion was used to describe its yield behavior.

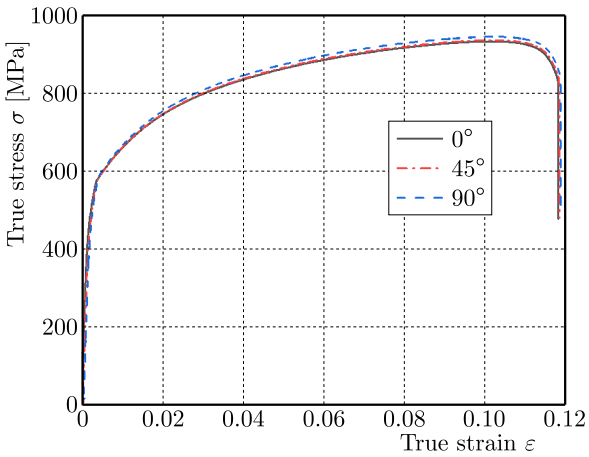


Fig. 2. The true stress-true strain curves of samples with different orientations

### 2.3. Comparison of DP780 hardening models

An accurate description of the hardening behavior of materials before fracture is the key to calibrating the parameters of the ductile fracture criterion. During the deformation of the specimen, the fracture strain is often higher than the maximum uniform strain, so it is necessary to establish a suitable hardening model to accurately predict the flow stress of the material in a large plastic strain range. In this paper, the classical Swift unsaturated hardening model (Swift, 1952) and the Voce saturated hardening model (Voce, 1948) are selected to characterize the hardening behavior of the DP780 sheet. The von Mises criterion based on constitutive relation matrix representation can be referred to in the literature (Ortiz and Simo, 1986). The hardening models are shown in Eq. (2.2) and (2.3), respectively

$$\sigma = K(\varepsilon_0 + \overline{\varepsilon}_p)^n \tag{2.2}$$

where $K$ is the hardening coefficient, $n$ is the hardening exponent, $\varepsilon_0$ is the initial yield strain and $\overline{\varepsilon}_p$ is the equivalent plastic strain.

Compared with the Swift model, the Voce model fully considers the effect of the initial yield point on the flow stress, and the stress will constantly approach the saturation state under large strain conditions, which means that the stress-strain curve will exhibit horizontal asymptotes, which can prove the constitutive relationship of metal materials under large strain conditions

$$\sigma = \sigma_0 + A(1 - exp(-c\overline{\varepsilon}_p)) \tag{2.3}$$

where $A$ and $c$ are material constants and $\sigma_0$ is the saturation stress.

The transformation equation of the true stress-true strain curve and true stress-plastic strain curve is given by

$$\overline{\varepsilon}_o = \varepsilon - \frac{\sigma}{E} \tag{2.4}$$

where $E$ is the elastic modulus.

The real stress-plastic strain test curve of the tensile specimen at 0° with the rolling direction in the uniform deformation section is shown in Fig. 3.

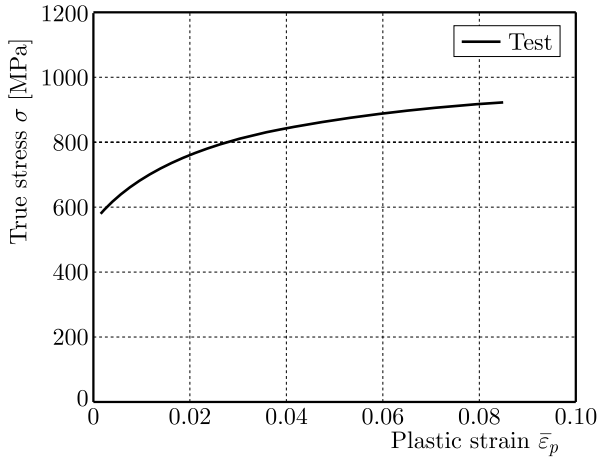


Fig. 3. True stress-plastic strain curve

Through the least square method, the Swift and Voce model parameters can be obtained from the true stress-plastic strain curve, as shown in Table 2.

**Table 2.** Hardening model parameters

| Parameter | $K$ [MPa] | $\varepsilon_0$ | $n$ | $\sigma_0$ [MPa] | $\sigma_s$ [MPa] | $A$ [MPa] | $c$ |
|---|---|---|---|---|---|---|---|
| Value | 1388 | 0.004 | 0.157 | 570 | 584.59 | 357.1 | 34.8 |

To verify the accuracy of the two hardening models for the characterization of the plastic behavior of the DP780 sheet, the von Mises yield criterion and the VUMAT subroutine of the two hardening models are compiled by the Fortran language. The compiled subroutine is embedded in Abaqus to simulate the tension process of uniaxial tensile specimens through the finite element method (FEM). A comparison of the simulation and experiment is shown in Fig. 4. It can be seen from Fig. 4a, both Swift and Voce hardening models can accurately describe the hardening behavior of DP780 specimens in the uniform plastic zone. From Figs. 4a and 4b, the Voce model underestimates the flow stress of DP780 in a large strain range, however, the Voce model cannot accurately predict the stress in a large strain range. While the Swift model slightly overestimates the flow stress in a large strain range, but still accurately describes the stress of DP780 in that range. Therefore, the Swift hardening model is selected to describe the hardening behavior of the DP780 specimen in a uniform plastic zone.

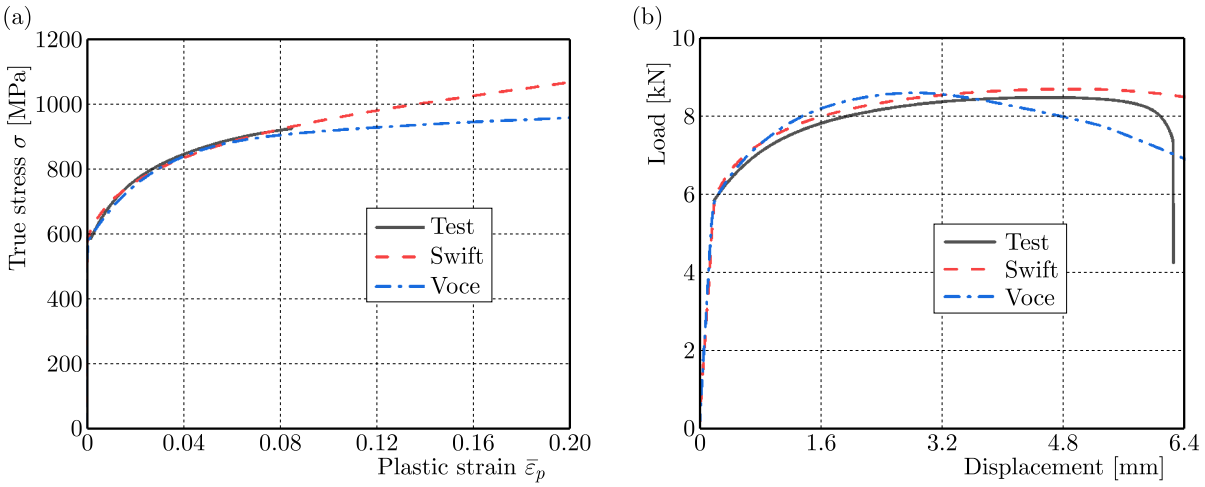


Fig. 4. Comparison of the simulation and test curves obtained by using two hardening models: (a) comparison of true strain-plastic strain curves, (b) comparison of load-displacement curves

Unidirectional loading tests of pure shear and tensile shear specimens with different notch angles can only find load-displacement curves in order to obtain stress parameters and fracture strain at the notch. Hence, corresponding simulations are performed to further verify the accuracy of the von Mises yield criterion and the Swift hardening model for predicting the plastic behavior of DP780 sheets before fracture. When the load-displacement curve of the FEM simulation is in good agreement with the test, the stress parameters and fracture strain at the moment of fracture of each sample can be obtained.

The S4R shell element is used in the finite element model of the tension-shear specimen to ensure simulation accuracy and computational efficiency. The S4R element has high simulation accuracy in large strain simulation and a wider scope of application (Luo and Wierzbicki, 2010). The grids of the central ligament area of the sample with large plastic deformation are refined, and the refined grid size is 0.08 mm. A comparison of FEM simulated and test load-displacement curves are shown in Fig. 5. The von Mises yield criterion and Swift hardening model well characterize the plastic behavior of DP780 tensile-shear specimens before fracture, which can be used to calibrate the ductile fracture criterion.

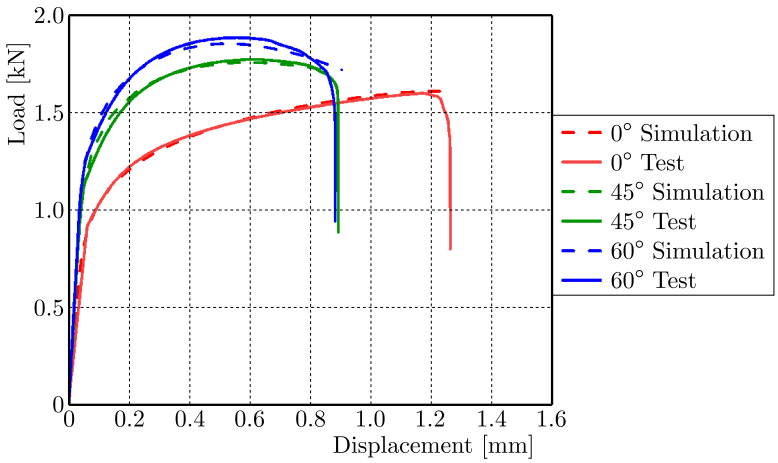


Fig. 5. Comparison of simulation and test load-displacement curves of tensile-shear specimens with different notch angles

## 3. Parameter calibration of the ductile fracture criterion and prediction of the tensile-shear test of DP780 sheet

### 3.1. Ductile fracture criterion including stress triaxiality and the Lode parameter

The stress triaxiality and Lode parameter are the determining factors affecting fracture initiation of the sheet. Therefore, the three criteria of Lou-Huh (Lou *et al.*, 2012), Cockcroft--Latham (Cockcroft and Latham, 1968), and Rice-Tracey (Rice and Tracey, 1969) are applied to the shear fracture prediction of the DP780 sheet. The expressions of the three criteria are shown in Table 3.

**Table 3.** Expressions of relevant ductile fracture criteria

| Ductile fracture criterion | Expressions |
|---|---|
| Lou-Huh | $\int_0^{\overline{\varepsilon}_f} \left(\frac{2}{\sqrt{L^2+3}}\right)^{a_1} \left(\frac{\langle 1+3\eta\rangle}{2}\right)^{a_2} d\overline{\varepsilon}_p = a_3$ |
| Cockcroft-Latham | $\int_0^{\overline{\varepsilon}_f} \sigma(\overline{\varepsilon})^* \left(\eta + \frac{3-L}{3\sqrt{L^2+3}}\right) d\overline{\varepsilon}_p = b$ |
| Rice-Tracey | $\int_0^{\overline{\varepsilon}_f} 0.283 \exp\left(\frac{3\eta}{2}\right) d\overline{\varepsilon}_p = c$ |

### 3.2. Parameter calibration of three ductile fracture criteria

In this paper, pure shear specimens, 45° and 60° tensile shear specimens are selected to calibrate the fracture criterion parameters. It is difficult to directly obtain the state parameters such as stress triaxiality $\eta$, Lode parameters $L$, and fracture strain $\overline{\varepsilon}_f$. Consequently, based on the hardening model selected in Table 3, the ductile fracture criterion is calibrated by a combination of the test method and FEM simulation. Since the initial fracture time of the specimen cannot be accurately determined during the test, the moment when the load-displacement curve drops sharply is equivalent to the initial fracture time, and the displacement $d$ corresponding to the fracture time is taken as the fracture displacement. The elements with the maximum equivalent plastic strain in the ligament region at the fracture time are selected as the initial fracture elements. The equivalent plastic strain value of these initial fracture elements at the initial

fracture time is taken as the fracture strain. The variation curves of the stress triaxiality and Lode parameter with the equivalent plastic strain $\bar{\varepsilon}_p$ of initial fracture elements are shown in Fig. 6.

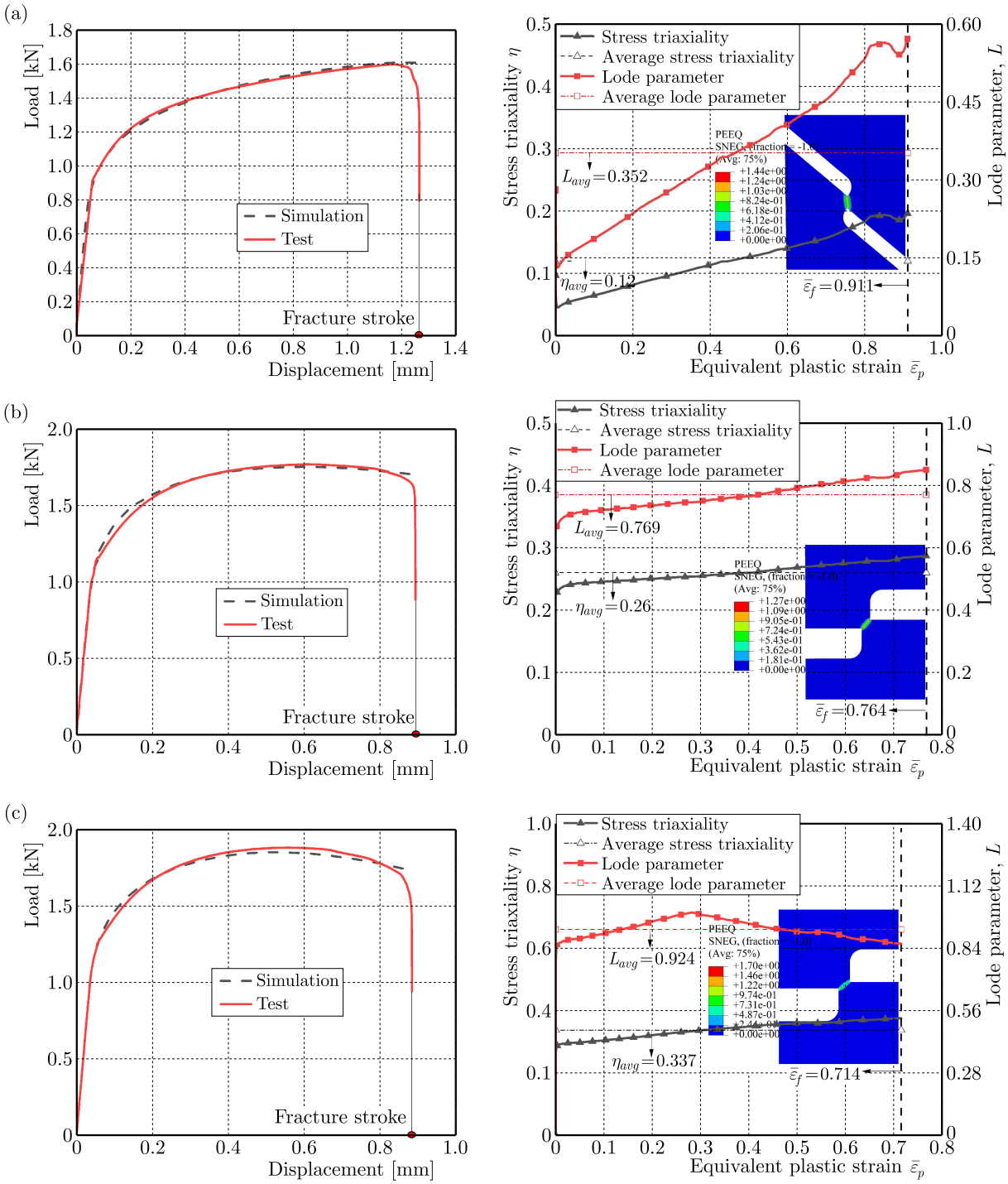


Fig. 6. The stress triaxiality and Lode parameter change curve of tensile-shear specimens with different notch angles: (a) pure shear specimen, (b) 45° tensile-shear specimen, (c) 60° tensile-shear specimen

The stress triaxiality and Lode parameters vary with the equivalent plastic strain $\bar{\varepsilon}_p$, which cannot be directly substituted into the fracture criterion to solve the fracture parameters. According to Eqs. (3.1), the stress triaxiality $\eta$ and lode parameters $L$ in the whole process of

stress change are averaged to obtain the average stress triaxiality $\eta_{avg}$ and average Lode parameters $L_{avg}$ (Qian *et al.*, 2020)

$$\eta_{avg} = \frac{1}{\overline{\varepsilon}_f} \int_0^{\overline{\varepsilon}_f} \eta(\overline{\varepsilon})\, d\overline{\varepsilon}_p \qquad L_{avg} = \frac{1}{\overline{\varepsilon}_f} \int_0^{\overline{\varepsilon}_f} \theta(\overline{\varepsilon})\, d\overline{\varepsilon}_p \tag{3.1}$$

where $\eta_{avg}$ is the average stress triaxiality, $L_{avg}$ is the average Lode parameter, and $\overline{\varepsilon}_f$ is the fracture strain. The calculated fracture state parameters are shown in Table 4.

**Table 4.** Parameters of the fracture state

| Specimen type | Fracture displacement | Fracture strain | Stress triaxiality | Lode parameter |
|---|---|---|---|---|
| Pure shear | 1.25 mm | 0.911 | 0.08 | 0.352 |
| 45° tensile-shear | 0.88 mm | 0.764 | 0.26 | 0.764 |
| 60° tensile-shear | 0.85 mm | 0.714 | 0.337 | 0.714 |

The stress and strain state parameters in Table 4 are respectively substituted into the expression for the fracture criterion in Table 3 to obtain equations with undetermined fracture criterion parameters. The fracture criterion parameters are calculated by solving the equations, as shown in Table 5.

**Table 5.** Calibrated fracture criterion parameters

| Ductile fracture criterion | Parameter 1 | Parameter 2 | Parameter 3 |
|---|---|---|---|
| Lou-Huh | 3.32 | 1.5128 | 0.7658 |
| Cockcroft-Latham | 0.3067 | – | – |
| Rice-Tracey | 1312 | – | – |

### 3.3. Tension-shear fracture prediction by three criteria

The tensile-shear test is simulated by using the three calibrated fracture criteria, and the fracture morphologies of the experimental and simulated samples are consistent. It can be seen from Fig. 7 that the fracture section of the sample is relatively flat with obvious shear slip bands. The fracture surface is gray and suede, and the fracture is full of dimples. The large notch angle of the fracture indicates that the shear part generates large plastic deformation under dislocation tension on both sides during loading, so the rotation effect occurs.

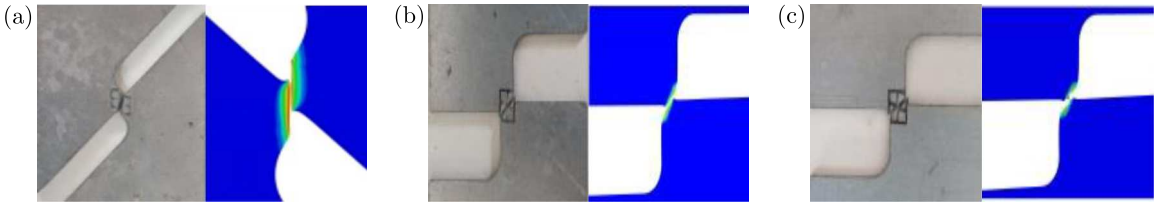


Fig. 7. Comparison of sample fracture morphology between the simulation and experiment: (a) pure shear specimen, (b) 45° tensile-shear specimen, (c) 60° tensile-shear specimen

In order to further verify the prediction accuracy of the ductile fracture criterion for fracture displacement of the tensile-shear specimen, the load-displacement curves of the test and FEM simulated tensile-shear fracture are compared as shown in Fig. 8. When the element fracture threshold of the finite element model of the specimens reaches 1, the corresponding elements are deleted to determine that the sheet begins to fracture.

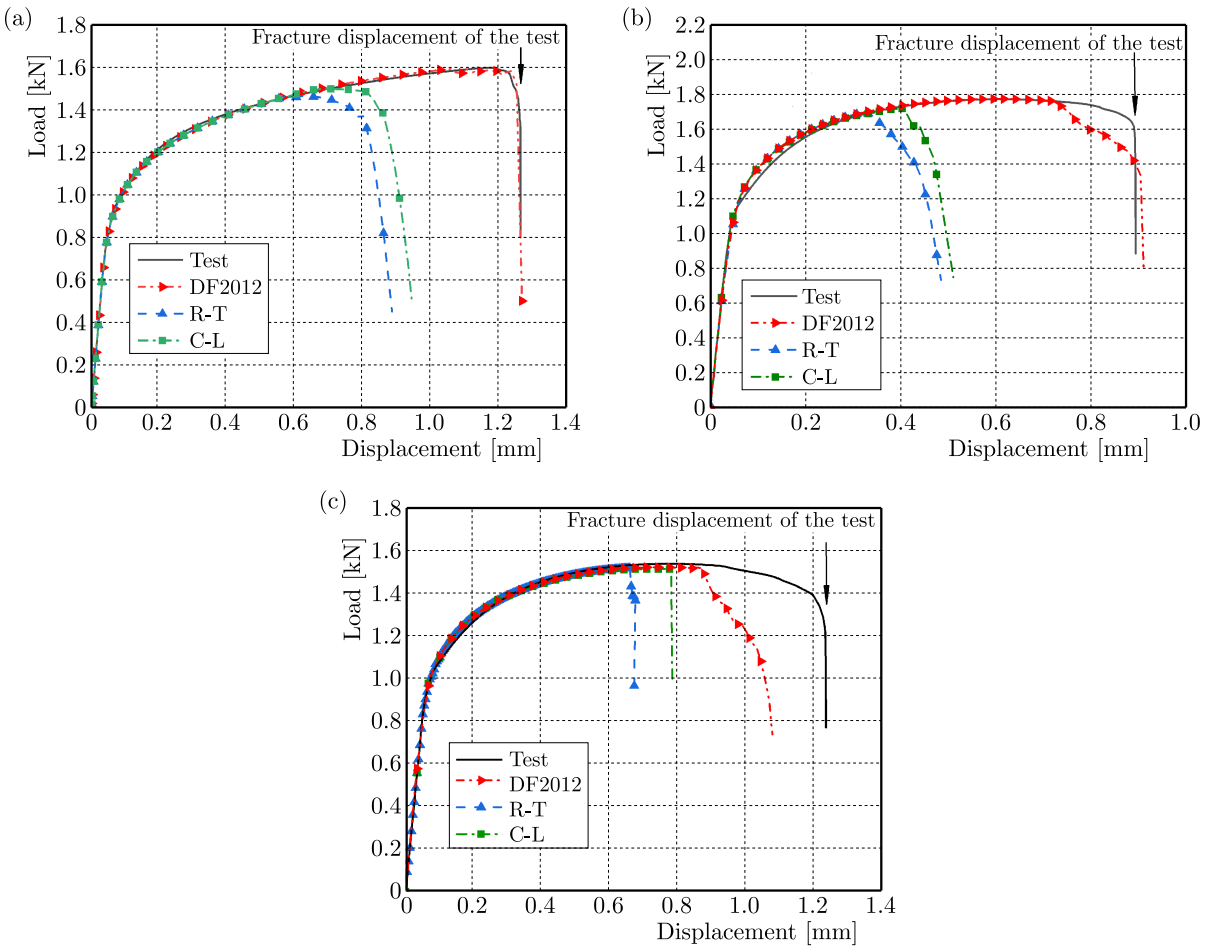


Fig. 8. Fracture displacement and test displacement of specimens with different notch angles: (a) pure shear specimen, (b) 45° tensile-shear specimen, (c) 60° tensile-shear specimen

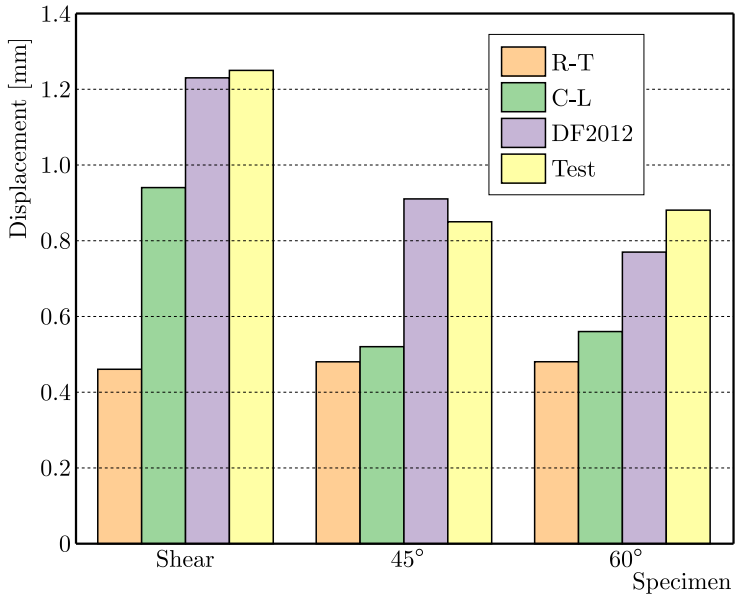


Fig. 9. Comparison of fracture displacement simulation values of various criteria

The fracture displacement values and test values of the specimens are summarized in Fig. 9. The Lou-Huh ductile fracture criterion can more accurately predict the fracture displacement of the specimens than the other two criteria, which indicates that the Lou-Huh ductile fracture criterion can be used to predict the tensile-shear fracture of the DP780 sheet in the low-stress triaxiality range (0.08-0.33). The reason for the accurate prediction of the Lou-Huh ductile fracture criterion is that both the stress triaxiality and the Lode parameter on material fracture are considered, and a more reasonable relationship between the fracture strain, stress triaxiality, and Lode parameter are constructed.

## 4. Application of the Lou-Huh criterion to shear fracture prediction in stretch bending of DP780 sheet

### 4.1. DP780 trough forming test

Relevant studies have shown that the blank holder force and the ratio of fillet radius to sheet thickness $t$ are the main technological factors affecting fracture behavior. The sheet is prone to shear fracture under a larger blank holder force or a smaller ratio of fillet radius to sheet thickness. The shear-dominated fracture in the low-stress triaxiality region is caused by continuous development of micro-cracks and micro-voids into shear bands under shearing action (Li *et al.*, 2011b).

Based on the precise prediction effect of the Lou-Huh ductile fracture criterion on the fracture behavior of tensile-shear specimens, a pull-bending forming shear fracture test of the DP780 sheet under the condition of a small ratio of fillet radius to sheet thickness and large blank holder force is designed. In addition, the Lou-Huh ductile fracture criterion is also applied to the forming FEM simulation to verify the fracture prediction accuracy of the Lou-Huh ductile fracture criterion by comparing the FEM simulation results with test results.

Figure 10 shows the trough mold for the pull-bending forming shear fracture test. The fillet radius at the entrance of the die is $R_{d1} = 2.5$ mm, and the gap between the die and the punch is $G = 1.1$ mm. During the test, the blank holder force remained unchanged, and the shear fracture behavior of the DP780 sheet under different bending fillet radii $R_p$ is observed by adjusting the bending fillet radius.

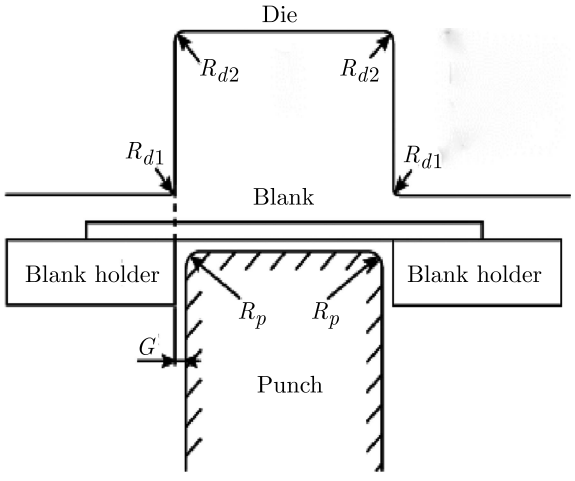


Fig. 10. Drawing and bending forming die size

The model of the test press is YZ32-160S, which is mainly composed of a die, punch, draw bead, and blank holder, as shown in Fig. 11a. The size of the trough sheet sample is 250 mm×30 mm×1 mm. The test process is as follows.

The sample is placed flat in the middle of the blank holder, and the die moves downward at a speed of 10 mm/s and contacts the sheet. At this time, the sheet is fixed between the die and the blank holder due to the blank holder force. Then the punch moves upward at a speed of 1 mm/s to push the sheet out and press the sheet into its concave die. When the sheet breaks, the punch stops moving. During the test, the test blank holder force is set to 185 kN, and the bending fillet radius of the die is adjusted by replacing the punch (1 mm, 3 mm, 5 mm) so that the DP780 sheet stamping exhibits shear fracture behavior at different small bending fillets of the punch.

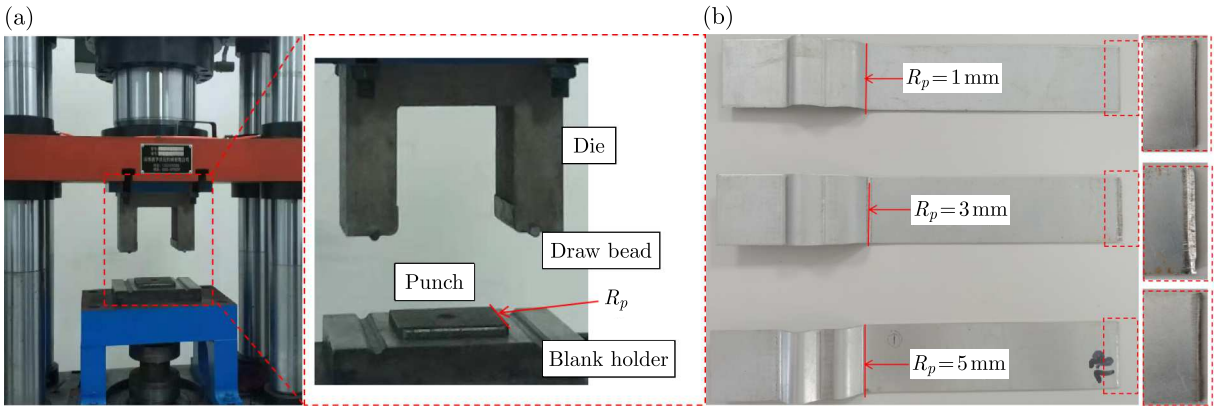


Fig. 11. Tension-bending fracture specimen

The DP780 sheet after stamping fracture is shown in Fig. 11b. A shear fracture of the DP780 sheet is generated at the bending fillet of the punch, the fracture is relatively flat without obvious necking, and the fracture is full of dimples of uniform size, which is similar to a brittle fracture. The reason for the brittle fracture is owing to the strength difference between martensite and ferrite in the dual-phase steel and a large number of micro-voids nucleated during the deformation process under the coupled action of tension and bending. However, the nucleation fails to grow sufficiently, so the material undergoes a cleavage fracture, and the fracture failure type of the sheet is basically the brittle failure (Luo and Wierzbicki, 2010).

Test data under different punch fillet radii are shown in Table 6. Under the condition that the blank holder force remains approximately constant, the forming depth before fracture gradually increases with an increase of the $R_p/t$ value, which indicates that the $R_p/t$ value is one of the technological factors affecting the fracture.

**Table 6.** Results of the stamping test

| $R_p/t$ | Forming depth | Stamping force | Fracture type |
|---|---|---|---|
| 1 | 7.5 mm | 185 kN | shear fracture |
| 3 | 8 mm | 179 kN | shear fracture |
| 5 | 11.4 mm | 184 kN | shear fracture |

### 4.2. Simulation of the stretch-bending forming test for DP780 trough samples

According to the actual size of the stamping die, a finite element model is established in Abaqus, in which the punch, die and the blank holder are both analytical rigid bodies, while the sheet sample is a deformable body calculated by the S4R shell element. The shell element size of the DP780 sheet is 0.8 mm, and the element size of other components is 2 mm. The friction coefficient of the contact surface between the DP780 sheet and the blank holder is set to 0.125. The compiled Lou-Huh criterion VUMAT subroutine is called during stamping simulation, and the specific material parameters are shown in Table 2. The forming depth results at the moment

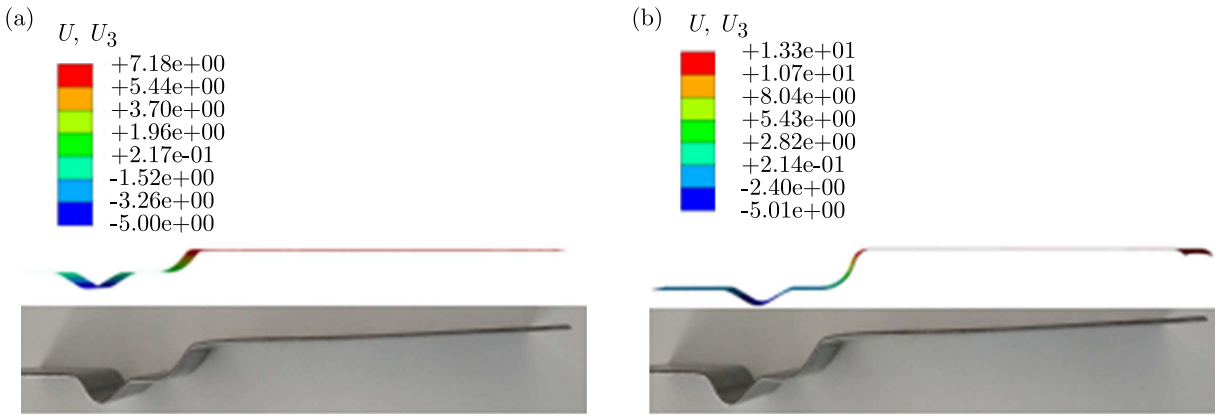


Fig. 12. Simulation and experimental values of forming depth under different punch fillets, the punch fillet radius is: (a) 1 mm, (b) 5 mm

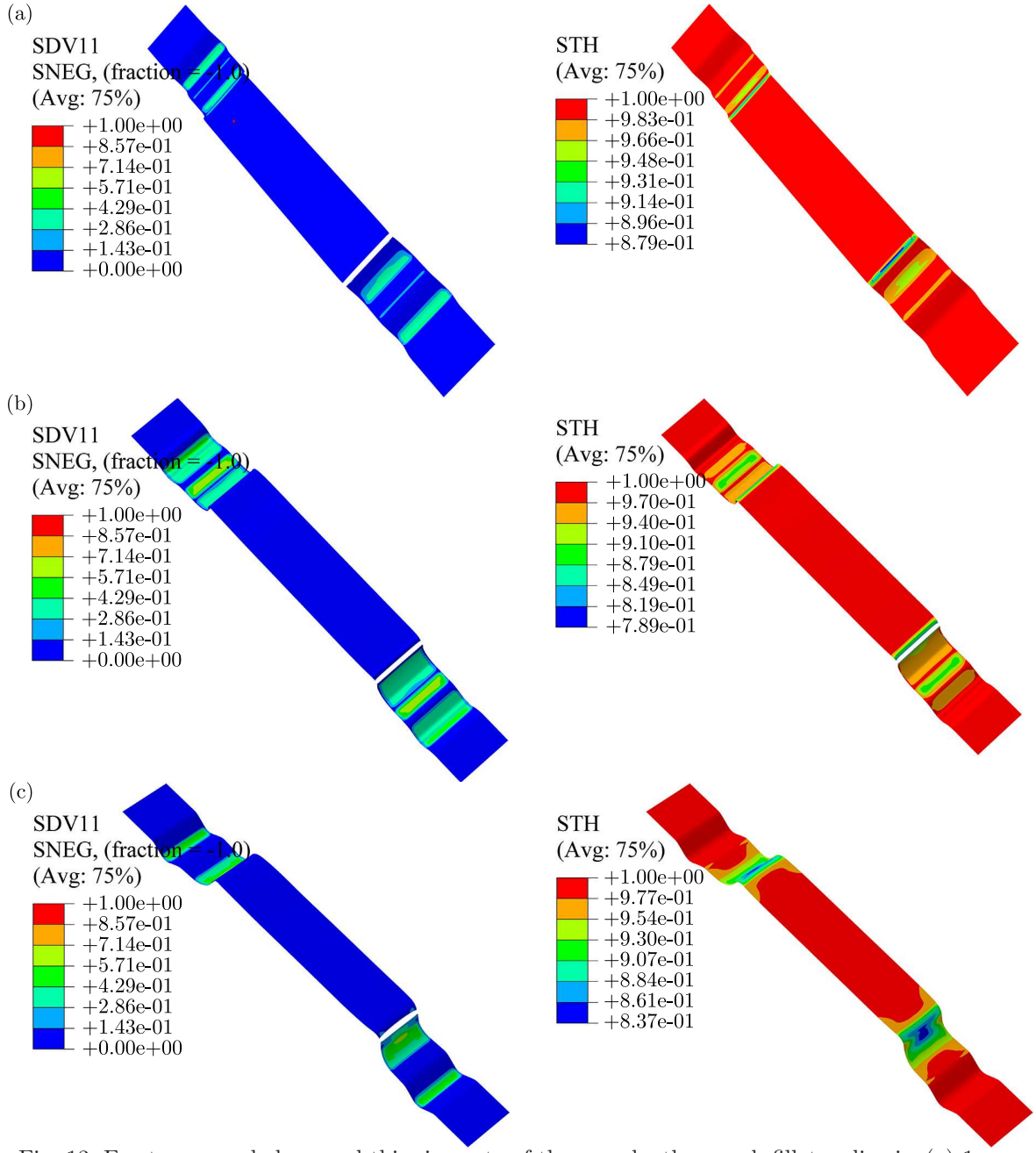


Fig. 13. Fracture morphology and thinning rate of the sample, the punch fillet radius is: (a) 1 mm, (b) 3 mm, (c) 5 mm

of sheet fracture during stamping simulation are extracted, and the simulated forming depth is compared with the test results, as shown in Fig. 12.

Different punch fillet radius values (1 mm, 3 mm, 5 mm) are used for stamping simulation to obtain the sheet fracture morphology and thinning rate data, as shown in Fig. 13. The fracture position of the simulated sheet is concentrated at the punch fillet, and the fracture section is flat without obvious necking. The maximum thinning rate at the moment of sheet fracture is only 10.4%, so the fracture type is a shear one.

The simulation results are compared with the test results as shown in Table 7. When $R_p = 1$ mm, the error between the test forming depth and the simulated forming depth is only 4.2%. When $R_p = 3$ mm, the corresponding error is a maximum of 9.5%. The results show that the Lou-Huh ductile fracture criterion can relatively accurately predict the shear fracture behavior at a small bending fillet of the die during the stamping process of the DP780 sheet.

**Table 7.** Comparison of simulation and experimental forming results

| $R_p/t$ | Simulated forming depth | Test forming depth | Thinning rate | Fracture type | Error |
|---|---|---|---|---|---|
| 1 | 7.5 mm | 7.18 mm | 10.4% | shear fracture | 4.2% |
| 3 | 8 mm | 8.76 mm | 9.3% | shear fracture | 9.5% |
| 5 | 11.4 mm | 10.7 mm | 9.4% | shear fracture | 6.2% |

## 5. Conclusion

Based on the uniaxial loading tests of four different specimens of advanced high-strength steel DP780, the hardening model of DP780 is studied first. The Lou-Huh, Cockcroft-Latham, and Rice-Tracey criteria for the ductile fracture are calibrated by the method of combining the test and FEM simulation, and the Lou-Huh criterion is used to predict the shear fracture of the DP780 sheet at a small bending fillet of the punch in the stretch-bending test. The specific conclusions are as follows:

- The Swift hardening criterion can accurately characterize the hardening behavior of the DP780 sheet before fracture. The Voce model can accurately predict the hardening behavior of DP780 sheets in uniform plastic sections, but it overestimates the flow stress of DP780 sheets under large strain conditions where the maximum error of the flow stress before fracture is more than 20%.
- Compared with the Cockcroft-Latham and Rice-Tracey criteria, the Lou-Huh ductile fracture criterion can more accurately predict the fracture behavior of DP780 tensile-shear specimens, and can more accurately predict the shear fracture of the DP780 sheet in the range of low-stress triaxiality (0.08-0.34). The results show that the combination of the Swift hardening law and Lou-Huh fracture criterion can provide accurate shear fracture prediction for the DP780 sheet metal.

*Fundings*

This work is supported by the National Natural Science Foundation of China under Grant (52302509, 52202512).

## References

1. Banabic D., Barlat F., Cazacu O., Kuwabara T., 2020, Advances in anisotropy of plastic behaviour and formability of sheet metals, *International Journal of Material Forming*, **13**, 749-787

2. Clift S.E., Hartley P., Sturgess C.E.N., Rowe G.W., 1990, Fracture prediction in plastic deformation processes, *International Journal of Mechanical Sciences*, **32**, 1, 1-17

3. Cockcroft M.G., Latham D.J., 1968, Ductility and the workability of metals, *Journal Institute of Metals*, **96**, 33-39

4. Hill R.T., 1952, On discontinuous plastic states, with special reference to localized necking in thin sheets, *Journal of the Mechanics and Physics of Solids*, **1**, 1, 19-30

5. Hu X., Wilkinson D.S., Jain M., Mishra R.K., 2009, The influence of particle shape, volume fraction and distribution on post-necking deformation and fracture in uniaxial tension of AA5754 sheet materials, *International Journal of Solids and Structures*, **46**, 13, 2650-2658

6. Li H., Fu M.W., Lu J., Yang H., 2011a, Ductile fracture: Experiments and computations, *International Journal of Plasticity*, **27**, 2, 147-180

7. Li M., Zhao Y.X., Hu X., Huang S., 2011, Experimental study of shear fracture on advanced high strength dual-phase steels, *Journal of Shanghai Jiaotong University*, **45**, 11, 1695-1699

8. Lou Y., Huh H., Lim S., Pack, K., 2012, New ductile fracture criterion for prediction of fracture forming limit diagrams of sheet metals, *International Journal of Solids and Structures*, **49**, 25, 3605-3615

9. Luo M., Wierzbicki T., 2010, Numerical failure analysis of a stretch-bending test on dual-phase steel sheets using a phenomenological fracture model, *International Journal of Solids and Structures*, **47**, 22-23, 3084-3102

10. Marciniak Z., Kuczynski K., 1967, Limit strain in the process of stretch-forming sheet metals, *International Journal of Mechanical Sciences*, **9**, 9, 609-620

11. McClintock F.A., Kaplan S.M., Berg C.A., 1966, Ductile fracture by hole growth in shear bands, *International Journal of Fracture Mechanics*, **2**, 614-627

12. Oh S.I., Chen C.C., Kobayashi S., 1979, Ductile fracture in axisymmetric extrusion and drawing – Part 2: Workability in extrusion and drawing, *Journal of Engineering for Industry*, **101**, 1, 36-44

13. Ortiz M., Simo J.C., 1986, An analysis of a new class of integration algorithms for elastoplastic constitutive relations, *International Journal for Numerical Methods in Engineering*, **23**, 3, 353-366

14. Puttick K.E., 1959, Ductile fracture in metals, *Philosophical Magazine*, **4**, 44, 964-969

15. Qian L., Ji W., Wang X., Sun C., Ma T., 2020, Research on fracture mechanism and prediction of high-strength steel sheet under different stress states, *Chinese Journal of Mechanical Engineering*, **56**, 24, 72-80

16. Rice J.R., Tracey D.M., 1969, On the ductile enlargement of voids in triaxial stress fields, *Journal of the Mechanics and Physics of Solids*, **17**, 3, 201-217

17. Silva M.B., Skjødt M., Atkins A.G., Bay N., Martins P.A.F., 2008, Single-point incremental forming and formability-failure diagrams, *The Journal of Strain Analysis for Engineering Design*, **43**, 1, 15-35

18. Swift H., 1952, Plastic instability under plane stress, *Journal of the Mechanics and Physics of Solids*, **1**, 1, 1-18

19. Voce E., 1948, The relationship between stress and strain for homogeneous deformation, *Journal of the Institute of Metals*, **74**, 537-562

20. Zhou X., Wang L., Fan Q., Liu S., 2021, Research on prediction method of rolling force for high strength steel in tandem cold rolling mill, [In:] *2021 China Automation Congress (CAC)*, 2398-2403

*Manuscript received July 2, 2023; accepted for print November 15, 2023*